Effect of Temperature and H Flux on the NH_3 Synthesis via Electrochemical Hydrogen Permeation

Ripepi, Davide; Schreuders, Herman; Mulder, Fokko M.

DOI
10.1002/cssc.202300460

Publication date
2023

Document Version
Final published version

Published in
ChemSusChem

Chemistry Europe
European Chemical Societies Publishing

WILEY VCH

Excellence in Chemistry Research

Announcing our new flagship journal

- Gold Open Access
- Publishing charges waived
- Preprints welcome
- Edited by active scientists

Meet the Editors of *ChemistryEurope*

Luisa De Cola
Università degli Studi di Milano Statale, Italy

Ive Hermans
University of Wisconsin-Madison, USA

Ken Tanaka
Tokyo Institute of Technology, Japan

ChemSusChem

Research Article
doi.org/10.1002/cssc.202300460

Chemistry Europe
European Chemical Societies Publishing

www.chemsuschem.org

VIP *Very Important Paper*

Effect of Temperature and H Flux on the NH_3 Synthesis via Electrochemical Hydrogen Permeation

Davide Ripepi,[a] Herman Schreuders,[a] and Fokko M. Mulder*[a]

Ammonia is an indispensable commodity and a potential carbon free energy carrier. The use of H permeable electrodes to synthesize ammonia from N_2, water and electricity, provides a promising alternative to the fossil fuel based Haber-Bosch process. Here, H permeable Ni electrodes are investigated in the operating temperature range 25–120 °C, and varying the rate of electrochemical atomic hydrogen permeation. At 120 °C, a steady reaction is achieved for over 12 h with 10 times higher cumulative NH_3 production and almost 40-fold increase in faradaic efficiency compared to room temperature experiments. NH_3 is formed with a cell potential of 1.4 V, corresponding to a minimum electrical energy investment of 6.6 kWh $kg^{-1}{}_{NH_3}$. The stable operation is attributed to a balanced control over the population of N, NH_x and H species at the catalyst surface. These findings extend the understanding on the mechanisms involved in the nitrogen reduction reaction and may facilitate the development of an efficient green ammonia synthesis process.

Introduction

With the increasing share in renewable energy generation, the electrification of large industrial chemical processes, such as the production of ammonia (NH_3), is considered a primary requirement to mitigate the climate crisis and reduce the dependency from fossil fuels. Electrocatalytic ammonia synthesis from dinitrogen (N_2) reduction is currently regarded as a potential alternative to the current energy intensive and environmentally impactful, fossil fuel powered, Haber-Bosch process.[1–4] Conventional aqueous electrochemical NH_3 synthesis appears extremely challenging, and the field is plagued with unreproducible results, due to mainly ammonia and nitrate impurity traces that obscure the dinitrogen reduction.[5–11]

Alternatively, an unconventional approach, based on hydrogen permeable electrodes, has been proven to be an attractive solution for the production of NH_3 from dinitrogen and water at ambient conditions.[12, include here as ref [13]: D. Ripepi, PhD thesis, Delft University of Technology (NL), **2023**. DOI: 10.4233/uuid:e75408f4-b1f3-446a-bfd5-19d9465f7038] This method uses a solid, non-porous, metal electrode to physically separate the electrochemical hydrogen generation from the catalytic dinitrogen activation and hydrogenation to ammonia. Because of this particular configuration, the two distinct catalytic surfaces can be independently optimised for the hydrogen generation and the nitrogen reduction, respectively. The approach harnesses the ability of certain reactive metal surfaces, like Ni, to spontaneously activate dinitrogen. This is possible when N_2 is not in competition with other adsorbate molecules, as hydrogen or oxygen species from the electrolyte.[13–17] The hydrogenation of adsorbed nitrogen is then carried out by atomic hydrogen generated from water electroreduction and permeating through the bulk of the solid metallic electrode. This design effectively limits and regulates the availability of H, which otherwise could dominate the catalytic interface in a conventional aqueous electrochemical environment, resulting in the suppression of N_2 activation.

Regrettably, the performance achieved using H permeable electrodes up to this point remains well below the metrics established by the US Department of Energy, aiming at a NH_3 production rate of 10^{-6} mol cm^{-2} s^{-1}.[18] One factor limiting the potential of this system is the decay in NH_3 yield rate observed after few hours of operation, indicating the occurrence of a deactivation process.[12] This mechanism is not yet well understood. However, a recent in situ study suggested that ambient temperature operation might be limited by slow N hydrogenation to NH and NH_3 desorption.[19]

On this basis, the present work provides a systematic investigation of the effect of operating temperature (in the range 25 to 120 °C, in which a concentrated 45 % *w/w* KOH solution can be used as liquid electrolyte) and H permeation flux on the N_2 reduction reaction, leading to a considerably improved NH_3 synthesis process.

Results and Discussion

In this study, a thin Ni foil is used as hydrogen permeable electrode. Ni is characterised by a weaker H interaction compared to other hydride forming metals (e.g., Pd), enabling lower hydride formation, which results in a negligible volume change upon H uptake. Moreover, since the H permeation rate

[a] *Dr. D. Ripepi, H. Schreuders, Prof. Dr. F. M. Mulder*
Materials for Energy Conversion and Storage (MECS), Chemical Engineering Department, Faculty of Applied Sciences
Delft University of Technology
Van der Maasweg 9, 2629 HZ Delft (The Netherlands)
E-mail: F.M.Mulder@tudelft.nl

Supporting information for this article is available on the WWW under https://doi.org/10.1002/cssc.202300460

is not yet limiting (i.e., permeating H flux is larger than the H consumption by NH_3 formation), the use of a different bulk electrode material with faster H permeation is considered not essential at this stage. In addition, dinitrogen activation on Ni is possible and results in the formation of surface nitrides with a suitable M–N bond strength.[12,20] Conversely, it was shown that other transition metals, such as Ru and Fe, do not perform better in the electrolytic cell configuration under investigation.[20]

Increasing the operating temperature results in a faster initial rate of NH_3 formation (Figure 1a). A deviation from an exponential trend (Arrhenius behaviour), indicates that temperature is involved in multiple different processes (catalytic and electrochemical) that take place in the studied nitrogen reduction reaction (NRR) using H permeable electrodes. The highest NH_3 yield rate of 2.5×10^{-12} mol cm^{-2} s^{-1} is obtained at 120 °C, corresponding to a 4-fold improvement compared to room temperature operation. The higher catalytic dinitrogen reduction is confirmed by alternating N_2 and Ar as feed gas, and through the reduction of purified $^{15}N_2$, while in operando measuring the production of gaseous ammonia with sensitive gas chromatography-mass spectrometry (GC-MS)[21,22] (Figures S3–S5 and Table S1). The $^{15}N_2$ is activated and reduced to $^{15}NH_3$, gradually replenishing the ^{14}N already present on the surface that when hydrogenated also forms $^{14}NH_3$ and makes N vacancies available for $^{15}N_2$ activation.

Remarkably, in addition to the pronounced enhancement in NH_3 yield rate, the increase in temperature has a beneficial impact on the stability of the reaction. This trend is clearly visualised in Figure 1b, where the amount of NH_3 produced is reported during 5 h experiments. Over time, at temperature below 120 °C, the ammonia production rate gradually declines, suggesting the occurrence of a deactivation mechanism. However, the latter appears to progressively vanish with increasing temperatures, until reaching a steady ammonia production at 120 °C. Long term experiments carried out at 120 °C reveal a constant yield rate and a total of 0.2 μmol of produced NH_3 after 12 h (Figure 1c and Figure S6). This is equivalent to 10 times larger cumulative NH_3 production, compared to our previously reported study (Figure 1c).[12] Multiple factors might be responsible for the observed trend. The deactivation mechanism occurring at lower temperatures might be related to the coverage dependence of activation barriers.[23–26] The adoption of an initial protective nitride layer results in a high starting N surface coverage.[12] However, as previously observed,[12] the depletion of N available at the Ni surface indicates that the rate of N replenishment is too sluggish. Therefore, as the N bond strength significantly

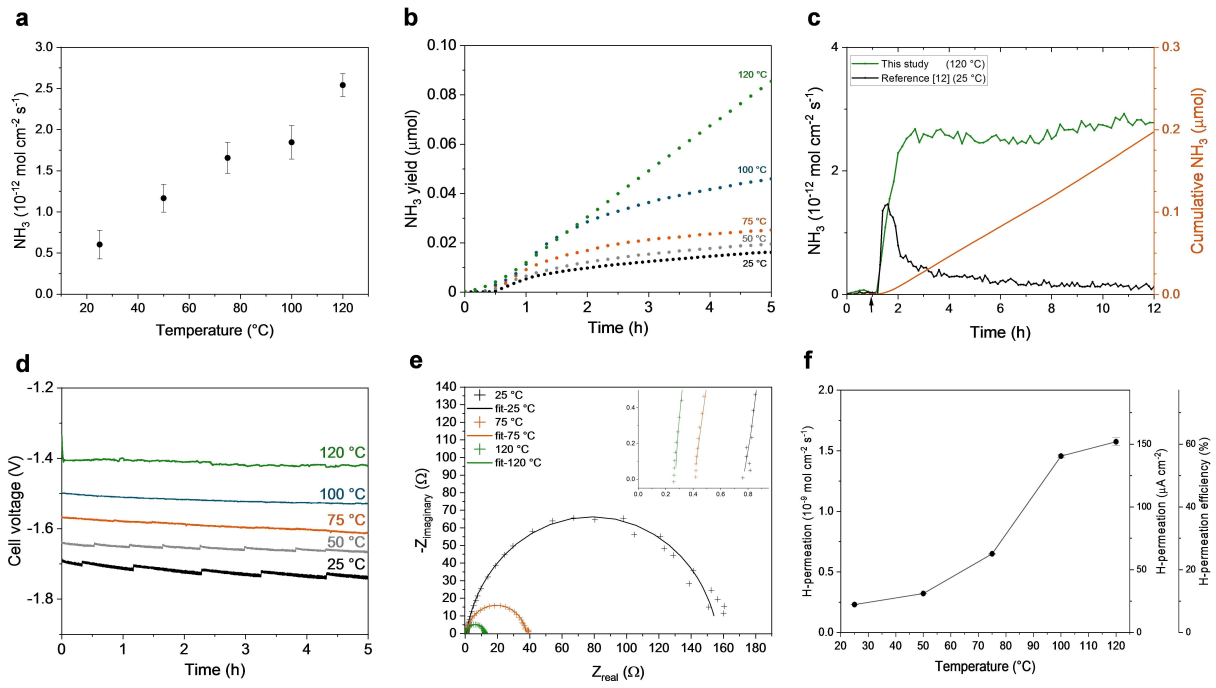

Figure 1. (a) Average ammonia production rate at different temperatures (during the first hour of measurement). Error bars indicate the standard deviation of three or more repeated independent measurements. (b) Cumulative ammonia production as function of time at different temperatures. (c) Long term experiments carried out at 120 °C from this study (green and orange lines) and at 25 °C from previous report[12] (black line). The arrow indicates the start of the cathodic charging. (d) Effect of the temperature on the cell potential recorded at a constant current density of 0.25 mA cm^{-2} (chronopotentiometry) over time. (e) Nyquist plot of electrochemical impedance spectroscopy measurements carried out at different temperatures. Symbols and solid lines indicate the measured values and the electronic equivalent circuit fittings respectively. The enclosure highlights the region of the Nyquist plot at the intersection of the impedance curve with the *x*-axis (real part of the impedance), which identifies the solution resistance. The experimental setup is shown in Figures S1 and S2. (f) Variation of the electrochemical hydrogen permeation flux as function of temperature reported in different units and permeation efficiency intended as ratio between the charging current density (0.25 mA cm^{-2}) and the rate of permeated hydrogen. The H-permeation efficiency is calculated on the basis of Equation (S2), and it is intended as ratio of the H atoms permeating through the Ni foil (forming H_2 or NH_3 at the solid-gas interface of the electrode) and the applied galvanostatic current density. More details are available in the Experimental Section of the Supporting Information.

increases with reducing N coverage,[24,27] the rate of the first hydrogenation (N to NH), which is considered the limiting step with the largest activation energy,[25] drops; slowing down the NH_3 synthesis.[20,26,27] Rising the operating temperature of several tens of degrees accelerates the rate of adsorption of nitrogen a few orders of magnitude.[23,28] Consequently, the enhanced nitrogen activation creates a more balanced catalytic cycle, maintaining apparently a constant N surface coverage through the NH_3 synthesis and N activation cycle. Additionally, higher temperatures promote the desorption of ammonia,[29–31] which can limit the availability of sites for dinitrogen activation at ambient temperature.

An increase in operating temperature accelerates the reaction kinetics and improves ionic conductivity and diffusion processes in (electro−)catalytic systems. As a result, the galvanostatic charging, applied for the generation of atomic hydrogen from water reduction, demands a lower cell potential at higher temperatures (Figure 1d). The cell potential represents the sum of the equilibrium potential and overpotential associated with multiple resistances.[32] Both the Gibbs free energy change (thus the equilibrium potential) and the overpotential of the overall water dissociation reaction decrease with the increasing temperatures.[32,33] The reduction of electrochemical resistances is measured by electrochemical impedance spectroscopy (EIS) measurements (Figure 1e). In the Nyquist plot, the intersection point of the impedance curve with the *x*-axis (real part of the impedance) identifies the solution resistance (R_s), which decreases from 0.78 Ω at room temperature, to 0.24 Ω at 120 °C (Figure 1e and Table 1). This is a direct consequence of the improved ionic conductivity of the KOH solution at higher temperatures.[34,35] At intermediate frequencies, the double layer capacitance and the charge transfer resistance (R_{ct}) are represented by a depressed semi-circle. The EIS results indicate an improved charge transfer rate as the operating temperature increases (Figure 1e and Table 1).

Ultimately, the temperature also affects the hydrogen transport rate through the electrode. It should be noted that, during electrochemical hydrogen permeation, only a fraction of the generated atomic hydrogen from water electroreduction (Volmer reaction) permeates through the electrode, while the remaining fraction recombines to H_2 via the Tafel or the Heyrovský reaction. The applied galvanostatic charging ensures that the atomic hydrogen formation rate at the electrode-electrolyte interface remains constant. However, the aliquot of permeated H sharply increases with temperature (Figure 1f), which is essentially associated with the temperature dependence of the hydrogen permeability (product of diffusivity and solubility).[36] An Arrhenius relationship correlates temperature and permeability;[37] however, deviations from the Arrhenius behaviour have been reported and are often attributed to surface effects.[38] Therefore, the temperature has a direct impact on the permeation efficiency, intended as ratio between the total hydrogen generated (i.e. equal to the galvanostatic current) and the permeated hydrogen. Other approaches to increase the electrochemical hydrogen permeation include the modification of the electrode bulk material (with higher H permeability),[39–41] the reduction of the electrode thickness,[42–44] or the adoption of H permeation promoters in the electrolyte.[45–50] We observed a substantial increase in hydrogen permeation efficiency, reaching 60 ± 2% at 120 °C (Figure 1f and Table S4). The following section will discuss the implications of enhanced hydrogen permeation on the overall reaction efficiency. An in-depth investigation and optimization on the electrochemical hydrogen permeation mechanisms fall out of the scope of the present work.

To evaluate the effect of the hydrogen permeation rate on the N reduction reaction under investigation, further experiments were carried out varying the charging current. Higher current densities result in faster H permeation, although at a lower permeation efficiency (Table S5). Consequently, the larger availability of reactive H at the catalytic surface increases the chance for hydrogenation of adsorbed N to NH, NH_2 and NH_3, thus accelerating the formation of NH_3 (Figure 2). However, the hydrogenation efficiency, defined as the ratio of the NH_3 synthesis rate (R_{NH_3}) and the atomic hydrogen permeation rate (H_{perm}), decreases at higher H_{perm}. This is because a larger aliquot of permeating H recombines at the side of the catalyst surface exposed to dinitrogen, indicating that the hydrogenation of adsorbed N is a slower process compared to the 2H recombination into H_2 on Ni. Furthermore, a too large H flux might result in the catalyst surface to be covered mostly by H/H_2, obstructing nitrogen adsorption, since direct competition for active sites has been observed.[12,16]

Table 1. Equivalent circuit model parameters applied for the fitting of the EIS measurements of Figure 1e using the Randel's circuit shown in Figure S7.

Temperature [°C]	R_s [Ω]	Constant phase element Q [F]	n	R_{ct} [Ω]
25	0.78	5.64×10^{-5}	0.899	156.6
75	0.41	5.95×10^{-5}	0.899	37.6
120	0.24	4.40×10^{-5}	0.899	12.0

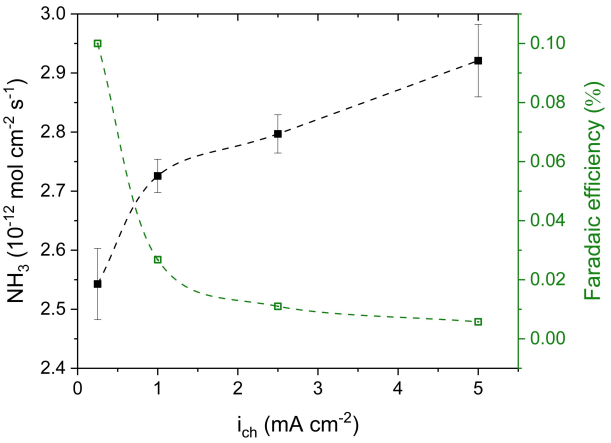

Figure 2. Ammonia production rate (black solid symbols) and faradaic efficiency (green open symbols) measured at 120 °C at different charging current densities. Error bars correspond to the standard deviation of three or more repeated independent measurements. Lines are a guide for the eyes.

Both the permeation and hydrogenation efficiency directly affect the faradaic efficiency (FE) of the overall process [Table S4 and S5 and Eqs. S1–S4]. Operating the electrolytic cell at 120 °C and 0.25 mA cm^{-2} results in almost 40-fold improvement in FE compared to our previous report.[12] Even though, so far, the overall FE for NH_3 remains fairly low (0.1 %, with the remaining 99.9 % assumed to be H_2), the produced NH_3 is formed with a cell potential of 1.4 V (Figure S6). This corresponds to an attractive practical minimum electrical energy investment of 6.6 kWh kg$^{-1}{}_{NH_3}$ for the electrochemical part of the process [Eq. (S4)]. Thus, the energy investment is substantially lower than the one required for either Haber-Bosch process (9.8 kWh kg$^{-1}{}_{NH_3}$) or lithium-mediated systems (14 kWh kg$^{-1}{}_{NH_3}$). The latter is to date regarded as potential electrochemical nitrogen reduction approach. Although recent works have demonstrated near unity selectivity,[51] as well as higher current densities (at the expense of a lower selectivity),[52] lithium-mediated systems intrinsically rely on a prohibitive Li plating potential (> 2.5 V vs. RHE),[53] scarce and expensive materials (i.e., Li and electrolytes),[54] and often on sacrificial ethanol as H source, while H_2 as proton source remains challenging and H_2O impractical, due to for example LiOH formation.[55] The use of either H_2 or ethanol adds to the total energy input of the process compared with starting from H_2O, as in the current manuscript.

Conclusion

The NH_3 synthesis using Ni hydrogen permeable electrode was investigated in the temperature range between 25 and 120 °C. Our results indicate that the increase in operating temperature considerably improves the NH_3 reaction rate, while also sustaining a stable catalytic cycle. This is possibly the result of enhanced nitrogen adsorption and NH_3 desorption, which maintain a steady N surface coverage throughout the NH_3 synthesis cycle, preventing the catalyst deactivation. Hence, to operate the nitrogen reduction reaction in a stable and efficient manner, a critical control over the population of N, NH_x and H species at the catalyst surface is necessary. Because of the adoption of H permeable electrodes, N activation and H permeation can be independently controlled, by a large extent, as shown here. Increased operating temperatures also favour a more efficient electrochemical hydrogen insertion, consequently leading to an increase in faradaic efficiency by a factor of 37 compared to the previous room temperature report,[12] as well as a lower electrical energy input.

Our investigation reveals a complex NH_3 synthesis mechanism resulting from the interplay of multiple processes involved in the electrolytic NH_3 production via electrochemical atomic hydrogen permeation. We anticipate that the scientific insights into the NH_3 synthesis mechanism and into the deactivation process will facilitate the design of suitable catalysts and the selection of operating conditions for the development of improved NH_3 yields.

Experimental Section

Materials

Polycrystalline nickel foil (Goodfellow, 99.9 % purity) with a thickness of 0.0125 mm was used as hydrogen permeable electrode. A nickel wire (MaTeck GmbH, > 99 % purity) with a diameter of 1 mm and total wetted geometrical area of about 5 cm^2 was used as counter electrode. The electrolyte was prepared by dissolving KOH (Sigma-Aldrich, 99.99 % purity) in MilliQ water with 45 % *w/w* concentration (solution boiling point 132.5 °C). Such concentrated electrolyte solution was necessary to operate the electrochemical cell at temperatures up to 120 °C and ambient pressure. High purity N_2 (Linde, 5 N) and Ar (Linde, 5 N), was used. Although the analysis for NO_x and NH_3 impurities, showed that the concentration of these contaminants in our feed gases did not exceed the lower detection limit (LOD_{NH_3}: 150 ppb, LOD_{NO_x}: 1 ppb), all the gases were cleaned with gas purifiers (Agilent OT3-4) prior introduction to the electrochemical cell, ensuring an efficient removal of all the possible NO_x and NH_3 contaminations.[12,56] This additional purification step was also applied to $^{15}N_2$ (99 atom % ^{15}N, Sigma-Aldrich) used for isotope labelled experiments, as $^{15}N_2$ might also contain traces of extraneous N species.[56,57]

Sample preparation

The sample preparation is analogous to the one carried out in our previous work.[12] In short, the Ni foil was cut with diameter of 28 mm and extensively cleaned with a Ar:H_2 plasma (7 : 1) for 30 min at 5 μbar, generated at 20 W RF power. Subsequentially, a protective surface nitride layer against oxidation[12,58] was generated by nitrogen plasma nitridation using an Ar:N_2 mixture (2 : 1) at 20 μbar and 40 W RF power for ten minutes. The stability of the Ni nitrided surface was tested at temperatures up to 150 °C under H_2, showing no formation NH_3 or N_2, thus underlining the benefit of the H permeable electrode.

Electrochemical setup

In this study, a two compartment electrochemical flow cell made of polyether ether ketone (PEEK) is used for all the electrochemical experiments. The 28 mm hydrogen permeable Ni electrode is fit into the electrochemical cell with a geometrical active area of 2.5 cm^2 (18 mm inner diameter). The hydrogen permeable Ni electrode separates the two sides of the electrochemical cell. In the liquid compartment side of the cell (1.6 mL), the electrolyte solution is circulated using a Masterflex peristatic pump (7 mL min^{-1}). In this compartment a Ni wire (5 cm^2) is used as counter electrode. At the other side, at the gas compartment (1.6 mL), the feed gas flow (1 mL min^{-1}, unless stated otherwise) is controlled by means of dedicated mass flow controllers (EL Flow Prestige – Bronkhorst). Silconert®2000 inert tubing was used for all the gas connections to minimize ammonia physisorption. All the NH_3 synthesis experiments were carried out using a Parstat MC 1000 potentiostat in galvanostatic conditions, with a constant charging current density of 0.25 mA cm^{-2}, unless otherwise stated.

This work focuses on the synthesis of NH_3 in the temperature range between 25 and 120 °C, which allows the use of concentrated liquid electrolyte (e.g., KOH). To operate at these temperatures, the electrochemical cell, a large electrolyte reservoir (150 mL), the PTFE tubing and Kapton insulated electric cables were installed inside a Carbolite PF Fan convection laboratory oven. Enough time was allowed for thermal equilibration of all the system components inside the oven. Prior to starting the electrochemical experiments, the temperature of the electrolyte reservoir was measured with a K-

Type thermocouple, to ensure the equilibration time was sufficient (±2 °C the setpoint temperature).

Gas analysis

Gas analysis was carried out in real time, connecting directly the outlet of the gas compartment of the electrochemical cell to the GC/GC-MS, without any external sample manipulation. An extensive description of the ammonia quantification methods via GC and via isotope sensitive GC-MS are available from our previous publications.[21,22] The hydrogen permeated and recombined to H_2 at the gas compartment side was quantified using a dedicated channel equipped with Hayesep N, Molsieve 5A and a thermal conductivity detector (TCD). A calibration curve for the H_2 quantification is provided in Figure S3. Unfortunately, due to the configuration of our system (Figure S1), it was not possible to reliably measure the H_2 produced in the liquid compartment.

Electrochemical impedance spectroscopy

Variations in ohmic, kinetic and mass transport resistance were identified and quantified using EIS. This technique has been widely applied to study various electrochemical processes.[59–61] The EIS measurements were performed with a VersaSTAT 4 potentiostat (AMETEK) at −1.6 V cell voltage (potentiostatic EIS) over a frequency ranges from 100 kHz to 0.2 Hz with an AC amplitude (w) of 10 mV.

The EIS measurements were fitted with a simple Randel's electronic equivalent circuit (Figure S7) using the ZView software. A constant phase element (CPE) replaces the double layer capacitor to account for the non-ideal capacitance behaviour, influenced by surface roughness, inhomogeneity, and porosity.[62,63] The CPE with impedance Z as a function of the applied angular frequency w is characterised by a pseudo-capacitance (Q) and a coefficient (n), as shown in Equation (1).[63]

$$Z = \frac{1}{(iwQ)^n} \quad (1)$$

Acknowledgements

This work is part of the Open Technology research program with Project Number 15234 which is (partly) financed by The Netherlands Organisation for Scientific Research (NWO).

Conflict of Interests

The authors declare no conflict of interest.

Data Availability Statement

The data that support the findings of this study are available in the supplementary material of this article.

[1] D. R. MacFarlane, P. V. Cherepanov, J. Choi, B. H. R. Suryanto, R. Y. Hodgetts, J. M. Bakker, F. M. Ferrero Vallana, A. N. Simonov, *Joule* **2020**, *4*, 1186–1205.
[2] R. Shi, X. Zhang, G. I. N. Waterhouse, Y. Zhao, T. Zhang, *Adv. Energy Mater.* **2020**, *10*, 2000659.
[3] R. F. Service, *Science* **2018**, *361*, 120–123.
[4] G. Soloveichik, *Nat. Catal.* **2019**, *2*, 377–380.
[5] M. Kolen, D. Ripepi, W. A. Smith, T. Burdyny, F. M. Mulder, *ACS Catal.* **2022**, *12*, 5726–5735.
[6] J. Choi, B. H. R. Suryanto, D. Wang, H.-L. Du, R. Y. Hodgetts, F. M. Ferrero Vallana, D. R. MacFarlane, A. N. Simonov, *Nat. Commun.* **2020**, *11*, 5546.
[7] S. Z. Andersen, V. Čolić, S. Yang, J. A. Schwalbe, A. C. Nielander, J. M. McEnaney, K. Enemark-Rasmussen, J. G. Baker, A. R. Singh, B. A. Rohr, M. J. Statt, S. J. Blair, S. Mezzavilla, J. Kibsgaard, P. C. K. Vesborg, M. Cargnello, S. F. Bent, T. F. Jaramillo, I. E. L. Stephens, J. K. Nørskov, I. Chorkendorff, *Nature* **2019**, *570*, 504–508.
[8] A. R. Singh, B. A. Rohr, J. A. Schwalbe, M. Cargnello, K. Chan, T. F. Jaramillo, I. Chorkendorff, J. K. Nørskov, *ACS Catal.* **2017**, *7*, 706–709.
[9] U. B. Shahid, Y. Chen, S. Gu, W. Li, M. Shao, *Trends Chem.* **2022**, *4*, 142–156.
[10] L. Hu, Z. Xing, X. Feng, *ACS Energy Lett.* **2020**, *5*, 430–436.
[11] M. Kolen, G. Antoniadis, H. Schreuders, B. Boshuizen, D. D. van Noordenne, D. Ripepi, W. A. Smith, F. Mulder, *J. Electrochem. Soc.* **2022**, *169*, 124506.
[12] D. Ripepi, R. Zaffaroni, H. Schreuders, B. Boshuizen, F. M. Mulder, *ACS Energy Lett.* **2021**, *6*, 3817–3823.
[13] Y. Abghoui, A. L. Garden, V. F. Hlynsson, S. Björgvinsdóttir, H. Ólafsdóttir, E. Skúlason, *Phys. Chem. Chem. Phys.* **2015**, *17*, 4909–4918.
[14] J. G. Howalt, T. Vegge, *Beilstein J. Nanotechnol.* **2014**, *5*, 111–120.
[15] H. Shi, K. Jacobi, G. Ertl, *J. Chem. Phys.* **1995**, *102*, 1432–1439.
[16] G. Ertl, M. Huber, S. B. Lee, Z. Paál, M. Weiss, *Appl. Surf. Sci.* **1981**, *8*, 373–386.
[17] G. Ertl, M. Huber, *Z. Phys. Chem.* **1980**, *119*, 97.
[18] G. Soloveichik, in *2019 AIChE Annual Meeting, AIChE*, **2019**.
[19] D. Ripepi, B. Izelaar, D. D. van Noordenne, P. Jungbacker, M. Kolen, P. Karanth, D. Cruz, P. Zeller, V. Pérez-Dieste, I. J. Villar-Garcia, W. A. Smith, F. M. Mulder, *ACS Catal.* **2022**, *12*, 13781–13791.
[20] D. Ripepi, B. Izelaar, D. van Noordenne, P. Jungbacker, M. Kolen, P. Karanth, D. Cruz, P. Zeller, V. Pérez-Dieste, I. J. Villar-Garcia, W. A. Smith, F. M. Mulder, *In preparation* **2022**.
[21] D. Ripepi, R. Zaffaroni, M. Kolen, J. Middelkoop, F. M. Mulder, *Sustain. Energy Fuels* **2022**, *6*, 1945–1949.
[22] R. Zaffaroni, D. Ripepi, J. Middelkoop, F. M. Mulder, *ACS Energy Lett.* **2020**, *5*, 3773–3777.
[23] J. J. F. Scholten, P. Zwietering, J. A. Konvalinka, J. H. de Boer, *Trans. Faraday Soc.* **1959**, *55*, 2166–2179.
[24] L. Diekhöner, H. Mortensen, A. Baurichter, A. C. Luntz, *J. Vac. Sci. Technol. A* **2000**, *18*, 1509–1513.
[25] G. Ertl, *Catal. Rev.* **1980**, *21*, 201–223.
[26] J. A. Dumesic, G. W. Huber, M. Boudart, in *Handbook of Heterogeneous Catalysis*.
[27] I. Chorkendorff, J. W. Niemantsverdriet, *Concepts of modern catalysis and kinetics*, John Wiley & Sons, **2017**.
[28] G. Ertl, S. B. Lee, M. Weiss, *Surf. Sci.* **1982**, *114*, 515–526.
[29] K. K. Al-Shammeri, J. M. Saleh, *J. Phys. Chem.* **1986**, *90*, 2906–2910.
[30] A. Chattopadhyay, H. Yang, J. L. Whitten, *J. Phys. Chem.* **1990**, *94*, 6379–6383.
[31] M. J. F. M. Verhaak, A. J. van Dillen, J. W. Geus, *Appl. Catal. A* **1993**, *105*, 251–269.
[32] A. J. Bard, L. R. Faulkner, *Electrochemical Methods: Fundamentals and Applications, 2nd Edition*, John Wiley & Sons, Incorporated, **2000**.
[33] S. A. Grigoriev, V. N. Fateev, in *Hydrogen Production Technologies*, **2017**, pp. 231–276.
[34] W. Feng, W. Pang, Y. Xu, A. Guo, X. Gao, X. Qiu, W. Chen, *ChemElectroChem* **2020**, *7*, 31–54.
[35] R. J. Gilliam, J. W. Graydon, D. W. Kirk, S. J. Thorpe, *Int. J. Hydrogen Energy* **2007**, *32*, 359–364.
[36] T. Otsuka, M. Shinohara, H. Horinouchi, T. Tanabe, *J. Nucl. Mater.* **2013**, *442*, S726-S729.
[37] S. Steward, "Review of hydrogen isotope permeability through materials; Lawrence Livermore National Lab. (LLNL), Livermore, CA (United States)", can be found under https://www.osti.gov/servlets/purl/5277693, **1983** (accessed 18 February 2022).
[38] D. S. Shupe, *J. Chem. Phys.* **1978**, *68*, 2612–2620.
[39] R. S. Delima, R. S. Sherbo, D. J. Dvorak, A. Kurimoto, C. P. Berlinguette, *J. Mater. Chem. A* **2019**, *7*, 26586–26595.

[40] H. Yukawa, T. Nambu, Y. Matsumoto, in *Advances in Hydrogen Production, Storage and Distribution* (Eds.: A. Basile, A. Iulianelli), Woodhead Publishing, **2014**, pp. 341–367.
[41] N. Boes, H. Züchner, *J. Less-Common Met.* **1976**, *49*, 223–240.
[42] V. Jayaraman, Y. S. Lin, *J. Membr. Sci.* **1995**, *104*, 251–262.
[43] M. H. A. Elhamid, B. G. Ateya, H. W. Pickering, *J. Electrochem. Soc.* **2000**, *147*, 2959–2963.
[44] A. L. Athayde, R. W. Baker, P. Nguyen, *J. Membr. Sci.* **1994**, *94*, 299–311.
[45] J. Flis, *Corrosion of metals and hydrogen-related phenomena: selected topics*, Elsevier, **2016**.
[46] J. Newman, L. Shreir, *Corros. Sci.* **1969**, *9*, 631–641.
[47] S. Qian, B. Conway, *Phys. Chem. Chem. Phys.* **1999**, *1*, 2805–2813.
[48] E. Akiyama, S. Li, *Corros. Rev.* **2016**, *34*, 103–112.
[49] M. Ichiba, K. Takai, J. i. Sakai, *ISIJ Int.* **2016**, *56*, 397–404.
[50] D. Dull, K. Nobe, *Corrosion* **1979**, *35*, 535–540.
[51] H.-L. Du, M. Chatti, R. Y. Hodgetts, P. V. Cherepanov, C. K. Nguyen, K. Matuszek, D. R. MacFarlane, A. N. Simonov, *Nature* **2022**, *609*, 722–727.
[52] K. Li, S. G. Shapel, D. Hochfilzer, J. B. Pedersen, K. Krempl, S. Z. Andersen, R. Sažinas, M. Saccoccio, S. Li, D. Chakraborty, J. Kibsgaard, P. C. K. Vesborg, J. K. Nørskov, I. Chorkendorff, *ACS Energy Lett.* **2022**, *7*, 36–41.
[53] O. Westhead, J. Barrio, A. Bagger, J. W. Murray, J. Rossmeisl, M.-M. Titirici, R. Jervis, A. Fantuzzi, A. Ashley, I. E. L. Stephens, *Nat. Chem. Rev.* **2023**, *7*, 184–201.
[54] C. Xu, Q. Dai, L. Gaines, M. Hu, A. Tukker, B. Steubing, *Commun. Mater.* **2020**, *1*, 99.
[55] H.-L. Du, K. Matuszek, R. Y. Hodgetts, K. Ngoc Dinh, P. V. Cherepanov, J. M. Bakker, D. R. MacFarlane, A. N. Simonov, *Energy Environ. Sci.* **2023**, *16*, 1082–1090.
[56] B. Izelaar, D. Ripepi, D. van Noordenne, P. Jungbacker, R. Kortlever, F. M. Mulder, *In Preparation* **2023**.
[57] R. Dabundo, M. F. Lehmann, L. Treibergs, C. R. Tobias, M. A. Altabet, P. H. Moisander, J. Granger, *PLOS ONE* **2014**, *9*, e110335.
[58] M. A. Z. Vasconcellos, R. Hinrichs, A. M. H. de Andrade, J. B. M. da Cunha, I. J. R. Baumvol, *Surf. Coat. Technol.* **2020**, *392*, 125753.
[59] X. Z. Yuan, C. Song, H. Wang, J. Zhang, *Electrochemical Impedance Spectroscopy in PEM Fuel Cells: Fundamentals and Applications*, Springer London, **2009**.
[60] M. A. Blommaert, D. A. Vermaas, B. Izelaar, B. in 't Veen, W. A. Smith, *J. Mater. Chem. A* **2019**, *7*, 19060–19069.
[61] Q.-C. Zhuang, X.-Y. Qiu, S.-D. Xu, Y.-H. Qiang, S. Su, in *Lithium Ion Batteries-New Developments*, (Ed. I. Belharouak) IntechOpen, **2012**, pp. 189–227, https://www.intechopen.com/chapters/29293.
[62] G. J. Brug, A. L. G. van den Eeden, M. Sluyters-Rehbach, J. H. Sluyters, *J. Electroanal. Chem. Interfacial Electrochem.* **1984**, *176*, 275–295.
[63] M. R. Shoar Abouzari, F. Berkemeier, G. Schmitz, D. Wilmer, *Solid State Ionics* **2009**, *180*, 922–927.

Manuscript received: March 31, 2023
Revised manuscript received: April 28, 2023
Accepted manuscript online: May 2, 2023
Version of record online: ■■, ■■

RESEARCH ARTICLE

Green ammonia: The effect of temperature on NH_3 synthesis using Ni hydrogen permeable electrodes was investigated. Increasing temperature improves the NH_3 production activity, efficiency and stability, thanks to the enhanced nitrogen adsorption and NH_3 desorption. Stable and efficient nitrogen reduction can be achieved by controlling the population of N, NH_x and H species at the catalyst surface.

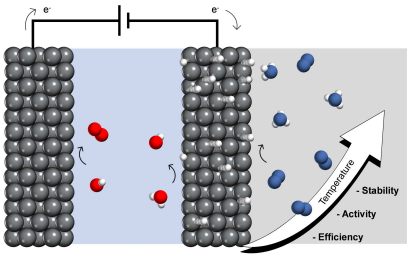

*Dr. D. Ripepi, H. Schreuders, Prof. Dr. F. M. Mulder**